Core-shell excitation of isoxazole at the C, N, and O K-edges – an experimental NEXAFS and theoretical TD-DFT study

T. J. Wasowicz[1*], I. Ljubić[2], A. Kivimäki[3,4], and R. Richter[5]

[1]Division of Complex Systems Spectroscopy, Institute of Physics and Applied Computer Science, Faculty of Applied Physics and Mathematics, Gdansk University of Technology, ul. G. Narutowicza 11/122, 80-233 Gdańsk, Poland http://orcid.org/0000-0001-5179-4021

*E-mail: tomasz.wasowicz1@pg.edu.pl

[2] Department of Physical Chemistry, Ruđer Bošković Institute, Bijenička cesta 54, HR-10000 Zagreb, Croatia https://orcid.org/0000-0002-3395-7293

[3] MAX IV Laboratory, Lund University, P.O. Box 118, 22100 Lund, Sweden

http://orcid.org/0000-0003-0753-8164

[4] Nano and Molecular Systems Research Unit, University of Oulu, P.O. Box 3000, 90014 Oulu, Finland

[5]Elettra – Sincrotrone Trieste, Area Science Park Basovizza, 34149 Trieste, Italy

http://orcid.org/0000-0001-8585-626X

Abstract

The near-edge X-ray absorption fine structure (NEXAFS) spectra of the gas-phase isoxazole molecule have been measured by collecting total ion yields at the C, N, and O K-edges. The spectral structures have been interpreted using the time-dependent density functional theory (TD-DFT) with the short-range corrected SRC2-BLYP exchange-correlation functional. Experimental and calculated energies of core excitations are generally in good agreement, and the nature of observed core-excitation transitions has been elucidated. The experimental C 1s, N 1s, and O 1s core electron binding energies (CEBEs) have additionally been estimated from another yield measurement where the neutral fragments in high-Rydberg (HR) states were ionized by the

electric field. For comparison, theoretical CEBEs have been calculated at the ΔM06-2X//mixed basis set level. We have also calculated the vibrationally resolved spectra pertaining to the lowest C 1s and N 1s core-excited roots in the Franck-Condon-Herzberg-Teller (FCHT) approximation. These spectra correlate well with the observed spectral features and have proven useful in resolving certain ambiguities in the assignment of the low-lying C 1s NEXAFS bands.

1. Introduction

Various fundamental compounds in diverse areas of chemistry, biology, and medicine comprise heterocyclic rings with oxygen and nitrogen heteroatoms. One of such bioactive molecules is isoxazole (C_3H_3NO, see Figure 1). It is a prototypical molecule due to its distinctive ring structure containing three regular sp^2 carbon atoms and oxygen and nitrogen atoms at adjacent positions connected via a fragile bond. In addition, an N=C bond is shorter than a C=C bond. Isoxazole has a fully conjugated set of π–electrons and exhibits pseudo-aromatic behavior. Isoxazole has thus specific electronic properties and chemical reactivity that cause, for example, unique photodissociation mechanisms[1] and the involvement of heteroatoms in strong hydrophilic interactions or coordinate bonds with ions[2].

Accordingly, isoxazole is embedded in many agrochemicals and pharmacological agents[2-5]. Isoxazole has become particularly important in the design of new drugs because numerous functional groups are readily attached to its scaffold, allowing the resulting compounds to interact with specific target proteins, such as the neurotransmitter agonist AMPA (α-amino-3-hydroxy-5-methyl-4-isoxazolopropionic acid) or microRNAs regulators[6, 7]. Such biological activities of isoxazole derivatives lead to reduced drug toxicity and the development of more effective clinical pharmacokinetics[2, 4, 7]. For this reason, isoxazole and its derivatives form the bioactive moieties of antibacterial, anticancer, antiviral, anti-microbial, antifungal, anti-

2

inflammatory, and anticonvulsant pharmaceuticals[4]. To understand the chemical reactivity and nature of chemical bonds, the ionization, excitation, and decomposition pathways of C_3H_3NO have recently been investigated utilizing theoretical and experimental methods[1, 8-16].

Despite the relevance of isoxazole in the synthesis of new pharmaceuticals and agrochemicals, the literature concerning its electronic structure is very sparse. Past studies of isoxazole mainly probed the UV-Vis absorption spectra of isoxazole, its excitation into the lower-lying ordinary states as well as higher-lying superexcited states[1, 8-10]. However, many fundamental physicochemical properties remain unexplored, especially concerning the core-shell excitation of isoxazole at the K-edges. To our knowledge, the C 1s, N 1s, and O 1s binding energies have not been determined experimentally for the gas-phase isoxazole molecule but only for a thin film of isoxazole on gold[17]. The molecular core binding energies have been calculated for isoxazole using density functional theory (DFT)[18, 19]. In the present work, we focus on interpreting the near-edge X-ray absorption fine structure spectra of the gas-phase isoxazole molecule measured at the C, N, and O K-edges. To aid in disentangling the spectral features, we have used the time-dependent density functional theory with the short-range corrected SRC2-BLYP exchange-correlation functional[20]. The relative intensities of experimental and TD-DFT modelled spectra are consistent. The experimental and theoretical energies of core-excitation transitions are in good agreement. The transition orbitals and oscillator strengths are calculated, which enable elucidation of the nature of observed core-excitation transitions. To complete the above results, we have determined the experimental and theoretical C 1s, N 1s, and O 1s core electron binding energies and the vibrationally resolved spectra of the lowest C 1s and N 1s core-excited roots in the Franck-Condon-Herzberg-Teller approximation.

2. Methods

2.1. Experimental

The NEXAFS spectra of isoxazole were measured using the total ion yield method at the Gas-Phase Photoemission beamline[21] at the Elettra synchrotron radiation facility in Trieste, Italy. A 36-period undulator produced synchrotron radiation that was monochromatized using a spherical grating monochromator equipped with a planar premirror. The storage ring operated in the multi bunch mode with a two ns interval between electron bunches. Five interchangeable gratings covered the beamline's operational range from 13.6 to 900 eV. The G4 grating was used to perform measurements at the C and N K-edges, while the G5 grating covered the energy range of the O K-edge.

The total ion yields and the yields of neutral high-Rydberg fragments of the isoxazole molecule were measured using a modified ion time-of-flight (TOF) spectrometer that has been described in the earlier publications[22, 23]. The TOF spectrometer contains a specific region that allows the detection of ions arising from field-ionized neutral HR fragments, while positive ions created in the interaction region – where the photon beam crosses the effusive beam of sample molecules – can be prevented from entering the ion TOF spectrometer by a suitable choice of potentials in the TOF spectrometer. A background contribution in the yield of field-ionized neutral HR fragments due to energetic photons and non-ionized metastable particles was measured with a different combination of potentials, see[23] for details. The instrument can also be employed to collect conventional total ion yields of positive ions from the interaction region.

Each NEXAFS spectrum was acquired in the vicinity of the particular ionization region by recording the ion yield signal with an MCP detector. Every spectrum was normalized to the photodiode current measured simultaneously. The photon energy was calibrated by measuring isoxazole NEXAFS spectra plus reference gases. In particular, the C 1s NEXAFS spectrum of isoxazole was energy calibrated according to the C 1s$\rightarrow\pi^*$ transition in CO_2 at 290.74 (4) eV[24].

Some N_2 and O_2 were found in the chamber due to a small leak in the gas inlet system. These residual gases did not alter the absorption features and were employed in the NEXAFS energy calibration. Therefore, the N 1s and O 1s NEXAFS spectra were calibrated according to the N 1s→π*, v=1 transition in N_2 at 401.10 (2) eV[24] and the O 1s→π* transition in O_2 at 530.8 (2) eV[25]. The photon energy resolution used in the NEXAFS measurements was estimated to be 30, 50, and 70 meV at the C, N, and O K-edges, respectively.

The sample of isoxazole was purchased from Sigma-Aldrich with a declared purity of 99%. Isoxazole is liquid at room temperature, and it was exposed to several freeze–pump–thaw cycles to remove the traces of residual gases. We did not heat the sample because isoxazole is volatile – its vapor pressure is 51.7±0.2 mmHg at 25°C[26]. An effusive beam of isoxazole vapor from a hypodermic needle was thus introduced into the interaction region, resulting in an ambient pressure of 2.4–4.2×10^{-6} mbar in the vacuum chamber during the measurements. The pressure in the interaction region was estimated to be 10–30 times higher.

2.2. Computational

The ground state minimum geometry and harmonic vibrational frequencies of isoxazole were computed at the spin-restricted MP2/cc-pVTZ level within the frozen core (FC) approximation[27,28]. The obtained MP2/cc-pVTZ minimum structure (see Electronic supplementary information – ESI) was subsequently used in the single-point calculations of the C 1s, N 1s, and O 1s core-electron binding energies (CEBEs), and the core-to-valence and core-to-Rydberg electronic excited states.

The CEBEs were computed in the ΔDFT formalism employing the Minnesota-styled hybrid meta-GGA M06-2X density functional[29] which previously showed a good performance in this context[30]. The singlet ground state and doublet C 1s, N 1s, and O 1s core-ionized densities for use in ΔDFT were converged at a mixed basis set level (denoted by //mixed), which was

5

initially proposed by Shim et al.[31] in the context of the ΔMP2 method. The //mixed consisted of the Peterson-Dunning's weighted core-valence triple-ζ cc-pwCVTZ[32] basis set on the C, N, or O atom whose core is ionized; model core potentials of the double-ζ polarized quality (mcp-DZP)[33] on the remaining second-row atoms; and the standard Dunning's double-ζ polarized cc-pVDZ basis set on the hydrogens[28]. The key feature of //mixed is that it contains only one 1s core orbital (due to the all-electron cc-pwCVTZ set) that is strictly localized on the atom of interest. This feature has thus far proved very advantageous for managing the SCF convergence to a desired core-hole state[30, 34]. The Aufbau structures of the core-hole states were successfully preserved by the maximum overlap method (MOM) algorithm[35]. The relativistic corrections of 0.10, 0.21, and 0.36 eV for C, N, and O atoms, respectively, were added a posteriori to the calculated ΔM06-2X CEBEs following the original recommendations[36].

To aid in the assignment of the core-to-valence and core-to-Rydberg NEXAFS transitions, we used the restricted single excitation space time-dependent DFT formalism (RSES-TD-DFT)[37] in the Tamm-Dancoff approximation.[38] For the RSES-TD-DFT computations we employed the short-range corrected SRC2-BLYP density functional[20] and the Pople-styled triple-ζ polarized basis set supplemented with two sets of diffuse functions, viz. 6-311(2+,2+)G**. The SRC2-BLYP/6-311(2+,2+)G** approach was specifically designed to accurately describe the K-edge spectra of molecules containing second-row atoms without the need for additional shifts in excitation energies[39]. Likewise, the TD-SRC2-BLYP oscillator strengths have repeatedly been found to correspond well to the intensities of the NEXAFS transitions[40]. Additional relativistic corrections to the TD-SRC2-BLYP core-excitation energies were not applied for the C, N, and O cores, in line with the original study[20]. For the C 1s core-excited states, the single excitations can be restricted to originate from only one C 1s core orbital at a time, or they may be allowed to mix by simultaneously exciting all three C 1s cores. We tested both these approaches; the former involved three independent TD-DFT runs with 30 roots per C atom, and the latter one TD-DFT

6

run with 90 requested roots. These numbers of roots were found to cover around 7 eV of the C 1s NEXAFS spectral range.

To model the vibrational fine structure in the NEXAFS spectra, we computed the vibronic intensities as the transition dipole moments (TDM) between the wave functions of the ground state and the lowest C 1s, N 1s, and O 1s core-excited states within the Franck-Condon-Herzberg-Teller approximation[41]. The MP2/cc-pVTZ geometry and unscaled harmonic vibrational frequencies were used to represent the ground state isoxazole. The lowest C 1s, N 1s, and O 1s core-excited structural minima and the corresponding (unscaled) harmonic vibrational frequencies were obtained from the root-specific TD-DFT optimizations performed at the $BH^{0.58}LYP$/6-311+G(2d,p) level. The $BH^{0.58}LYP$ density functional was designed with the HF exact exchange re-fitted to 58% to produce realistic core excitation energies and potential surfaces without the need for shifting and comparable to those of SRC2-BLYP[20]. The required TDMs are obtained from the same level of theory. The mixing between the normal modes of the ground and core-excited states was described via the full Duschinsky matrix[41]. The maximum quantum number for each mode and the maximum quantum number considered for the combination of modes were set to 30 and 20, respectively. The possibility of hot bands was not considered. No molecular point group symmetry was imposed in the optimizations of the core-excited minima.

The following quantum chemistry codes were used: Gaussian 16[42] (the MP2 ground state and TD-$BH^{0.58}LYP$ root-specific geometry optimizations; the vibrationally resolved spectra in the FCHT framework); GAMESS-US 2021 R1[43] (the computations of the CEBEs using the M06-2X//mixed approach), and Q-Chem 4.3[44] (the calculations of the NEXAFS spectra at the TD-SRC2-BLYP/6-311(2+,2+)G** level).

3. Results and Discussion

Neither the experimental NEXAFS nor theoretical spectra of isoxazole have been studied to the best of our knowledge. Thus, the C 1s, N 1s, and O 1s experimental NEXAFS and theoretical (TD-SRC2-BLYP/6-311(2+,2+)G**) core-excitation spectra of isoxazole are presented in the (a) panels of Figures 2–4. To facilitate the comparison, calculated TD-DFT spectra were scaled to display similar peak heights at the first resonance maxima with experimental NEXAFS spectra. Over the entire spectral range, we observed no transitions that would involve mixings of single excitations originating from different C 1s cores. Thus, the excitations calculated using one C 1s core at a time (3 × 30 roots) or three C 1s cores simultaneously in a single run (90 roots) produce identical SRC2-BLYP spectra.

The TD-SRC2-BLYP C 1s spectrum in Figure 2 is tentatively red-shifted by –0.50 eV. In doing so, our main goal was to achieve a better overlap between the experimental and theoretical spectral features in the lowest energy region where the first transitions from the three C 1s cores appear. These first bands are the strongest by far and pose a difficult problem to the present approach because they are apparently predicted as insufficiently resolved. This results in the erroneously predicted one strong peak and a shoulder where there should be two strong peaks with two shoulders (Figure 2). The involved TD-SRC2-BLYP peaks (after shifting by –0.5 eV) are centered at 285.75, 285.87, and 286.32 eV (Table 1); these respectively correspond to the lowest-lying and strongest transitions from the C4, C3, and C5 1s cores (for a full list of transitions and oscillator strengths see Table S2). The insufficient resolution of these transitions also causes spurious accumulation of the spectral intensity in the very narrow range resulting in comparatively poorer TD-SRC2-BLYP relative intensities (Figure 2).

For comparison, in the ESI (Figure S1) we also provide the TD-M06-2X vertical spectrum but this just lends further support to the observation that TD-DFT, even with the state-of-the-art density functionals, is not able to furnish an unambiguous assignment of the lowest

8

part of the C 1s NEXAFS. Some of these issues are successfully resolved by going beyond the vertical spectrum description and considering the detailed vibronic transitions (see Section 3.4).

A computer least-squares fitting procedure was applied to decompose the underlying excitation bands in the experimental NEXAFS spectra. The fits were performed for curves covering the energy ranges from the first resonances up to the $1s^{-1}$ ionization potentials. Gaussian functions were used to describe the shapes of the bands. The choice of Gaussian functions for modeling the NEXAFS spectra was dictated by the shape of the rising edges of the first resonance, which were reproduced in the fit with excellent accuracy by the Gaussian bands. Attempts were made to use other fitting functions, such as Lorentzian, which failed to reproduce the measured NEXAFS spectra. The vertical excitation energies of the bands in the NEXAFS curves obtained from the fittings (shown in the (b) panels of Figures 2-4) are listed in Tables 1-3. We estimate an overall accuracy of ±0.2 eV in determining the vertical excitation energies. Tables 1-3 also present calculated energies and assignments of the C 1s, N 1s, and O 1s core excited states of isoxazole. The ten lowest virtual orbitals used in these designations are depicted in Figure 5 using Molden software[45].

The experimental C 1s, N 1s, and O 1s CEBEs of the isoxazole molecule have been estimated from another yield measurement where we used the electric field to ionize neutral fragments in high-Rydberg (HR) states. Figure 6 displays high-Rydberg (HR) fragment yield measured at the K-edges of the isoxazole molecule (the red crosshair curves). The HR fragment yields were scaled to display a similar peak height at the first resonance maximum with an experimental NEXAFS spectrum. The HR fragment yields also include some "background" from soft X-ray and VUV photons, neutral fragments in metastable states, and those long-living Rydberg states for which field ionization was impossible. As seen in Figure 6, the "background" contribution (the navy blue dotted curve) is of minor importance.

9

As depicted in Figure 6, the HR fragment yields resemble the NEXAFS across the resonances. Indeed, both yields show the same core excitations, but a unique prominent feature appears in the HR fragment yields at higher photon energy. Similar features have been observed in other molecules using this technique[22, 23], where they are known to be located just above the core ionization threshold. The formation of this above-threshold maximum can be explained by the occurrence of ultrafast electron recapture processes induced by post-collision interaction between a slow photoelectron and a fast Auger electron in the field of the molecular ion[22, 46].

Since the appearance of the above-threshold maxima is connected to the corresponding IPs (only very slow 1s photoelectrons are efficiently recaptured), one can use their positions to estimate unknown core binding energies. For that purpose, we compared the well-known CEBEs with the fitted maxima of the above-threshold peaks observed in the studies of methane[22], carbon dioxide[23], dinitrogen[46], and water[47] molecules. We calculated that the IPs, on average, lie (230 ± 150) meV below the above-threshold maxima. So we estimated the core ionization energies of isoxazole using this approximation. The results are shown in Table 4. The uncertainties in the core electron binding energies are determined by combining all the sources of errors, i.e., those derived from the experimental peak positions (25 meV) and the fitting procedure (50 meV), and the correction factor uncertainty (150 meV). For comparison, the theoretical CEBEs have been calculated at the ΔM06-2X//mixed basis set level. These values and the results of other authors[17-19] are also shown in Table 4.

For completeness, we have calculated vibrationally resolved spectra of the lowest C 1s and N 1s core-excited roots in the Franck-Condon-Herzberg-Teller approximation. In order to produce the vibrationally resolved spectra in the FCHT framework, we carried out the state-specific optimizations of the lowest O 1s, N 1s, and C 1s core-excited roots at the TD-BH$^{0.58}$LYP/6-311+G(2d,p) level. The results are summarized in Table 5. The harmonic vibrational frequencies are reported in Table S1 of the ESI. Figures 7 and 8 show the

vibrationally resolved FCHT spectra corresponding to the lowest C 1s and N 1s roots and the assignments of the vibronic progressions according to the most important contributions. The enumeration of the harmonic frequencies follows Table S1 of the ESI. The vibrational modes that contribute most to the vibronic spectra are depicted in Figure 9. The peak widths in the vibrationally resolved theoretical spectra shown in Figures 7 and 8 do not include the broadenings by the intrinsic core hole lifetimes, not to complicate the interpretation of such structures. Theoretical spectra of the lowest C 1s and N 1s core excitations containing the convolution with typical half-widths due to the lifetimes are for completeness plotted in Figures S2 and S3 of the ESI.

3.1. C K-edge

The C 1s NEXAFS spectrum of isoxazole was measured in the 284-296 eV energy range with 25 meV steps (see Figure 2). As shown in Table 1, the vertical excitation energies of the bands in the C 1s NEXAFS spectrum obtained from the fittings and calculated energies (after the energy shift) are in reasonable agreement – inconsistencies are mostly lower than 0.3 eV.

The carbon K-edge NEXAFS spectrum of isoxazole presents the most intense peaks centered at 285.40, 285.83, and 286.39 eV. The three lowest core-excited states are predicted to contribute to this 285-287.0 eV region. In particular, each carbon atom exhibits an intense low-energy transition, which was calculated to lie at 285.75, 285.87, and 286.32 eV for the C4, C3, and C5 atoms, respectively. In all cases, these lowest-lying transitions correspond to the C(1s)$\rightarrow\pi^*$ excited state, which mixes excitations to two π^*(A") orbitals: 4a" (LUMO), which essentially consists of the N-O, C-N, and C-O antibonding interactions, and a somewhat higher-lying 5a" being predominantly the π^*(C-C) antibonding orbital (Figure 5). The contribution of the C(1s)$\rightarrow$4a" (LUMO) excitation always dominates the lowest core-excited state. This

11

excitation was predicted to be ~1.3–10 times more intense than the higher-lying C(1s)$\rightarrow\pi^*$ excited state dominated by the C(1s)$\rightarrow$5a'' excitation.

We used single Gaussian peaks in the simulations to fit these three resonances. However, a close-up on the 285-287 eV spectral region (see Figure 7) shows that these excitations reveal a well-separated vibrational fine structure (discussed further).

Each carbon atom produces two more intense excitations. One is the C(1s)$\rightarrow\pi^*$ core-valence transition, and the other is the C(1s)$\rightarrow$3s core-Rydberg transition with a small contribution of the in-plane $3p_y$ orbital (Figure 5; Table 1). The C(1s)$\rightarrow$3s($3p_y$) (A') core-Rydberg transition lies at a higher energy and is much less intense than the C(1s)$\rightarrow\pi^*$ transitions in the case of C3 and C4. In contrast, for the C5 carbon, the calculations predict the C(1s)$\rightarrow$3s($3p_y$) transition as the second-lowest lying and the second most intense transition. The vicinity of C5 to the O atom probably causes such inversion of transitions. Indeed, the diffuse 3s orbital density should be the most compact around the oxygen. It is recognized that the most significant contribution to the transition dipole moment (TDM) matrix element comes only from the electron density in the close vicinity of the atom in question because of the strict localization and compactness of the 1s core orbitals.

It should be noted that some relatively small wiggles in the experimental NEXAFS spectrum lying around 290.9-291.5 eV were reproducible during several measurements, so they are real structures (see Figure S4 and Table S3 of the ESI).

From the yields of high-Rydberg fragments, we have determined the CEBEs for the C3 $1s^{-1}$, C4 $1s^{-1}$, and C5 $1s^{-1}$ to be at 292.0, 291.1, and 292.5 eV, respectively. The C 1s core electron binding energies of isoxazole have also been calculated at the ΔM06-2X//mixed basis set level and listed in Table 4. The results of the calculations and those obtained from our gas-phase experiment are in good agreement. The experimental chemical shift between the C4 and

C3 carbon environments is 0.9 eV, while that between the C4 and C5 is 1.4 eV. The corresponding chemical shifts obtained from the calculations are 0.85 and 1.55 eV, respectively.

The only measurements of the CEBEs available in the literature for comparison come from studying the samples as thin films of isoxazole on gold[17]. The results of these earlier studies are about 5 eV lowered concerning our gas-phase values due to the surface work function and relaxation effects[48].

The isoxazole's core electron binding energies have also been calculated using density functional theory[18]. These results are slightly higher than our CEBEs but are still in very good agreement.

3.2. N K-edge

The N 1s NEXAFS spectrum of isoxazole was measured in the 398-416 eV energy range with 50 meV steps (see Figure 3). As shown in Table 2, the vertical excitation energies of the bands in the N 1s NEXAFS spectrum obtained from the fittings and calculated energies are also in good agreement. It is of note that there was a small leak in the gas inlet system so that the N(1s)→π*, $v = 0$-2 transitions of the N_2 molecule are visible in Figure 3 as three narrow structures at 400.88, 401.10, and 401.33 eV superimposed on the high-energy falling slope of the first resonance of isoxazole. The energy calibration was done according to these transitions.

The TD-SRC2-BLYP calculation indicates only two very intense core transitions, although their ordering by the intensity seems to be erroneously predicted. The first transition at 400.38 eV can be correlated to the first experimentally observed band, whose asymmetry hints at a fine structure. Thus, this band was fitted with two Gaussian peaks: 400.19 and 400.52 eV, which cover features of the vibrational fine structure of this excitation (see Figure 8). According to calculations, the 400.38 eV band corresponds to the N(1s)→π* transition dominated by the N(1s)→4a'' (LUMO) excitation.

13

The second theoretical transition at 403.14 eV can be correlated with the experimental 402.94 eV centered jagged broad absorption. This transition corresponds to a complex mix of excitations of the 3d and higher Rydberg orbitals. As seen in Table 2, six of the single excitations are reported to have a significant weight. Interestingly, the core-excited states corresponding to the transitions to the 3s and 3p Rydberg orbitals are found somewhat higher and are predicted to have only minor intensities. This observation differs from what is calculated for the C 1s spectrum.

We note, however, that the general uncertainties seen in the predictions of the Rydberg regions of the NEXAFS spectra (Figure 2-4) could be due to the use of the 6-311(2+,2+)G** basis set. The reason is that the positions and especially intensities of the Rydberg transitions are known to be predicted more reliably if special molecular Rydberg basis sets are used as opposed to the atom-centered diffuse functions found in standard basis sets[49]. This is also the reason why MOs built from atom-centred diffuse functions can sometimes be rather difficult to relate to the conventional ("hydrogen-like") Rydberg orbitals designated as 3s, 3p, 3d, etc. Part of the problem with the relative intensities could also lie in the use of the Tamm-Dancoff approximation to the full TD-DFT formalism[50].

The N(1s)→π* transition dominated by the N(1s)→5a" excitation also has noteworthy intensity. It is predicted to occur at 404.16 eV and is attributed to the shoulder observed at 403.96 eV on the high-energy flank of the widest spectral feature.

The experimental spectrum also exhibits intense peaks at 404.73, 405.01, and 405.52 eV, which are not reproduced in our calculations. These peaks compose resonances that may be similar to the peaks observed in the N K-edge spectra of five azabenzenes at around 403 eV[51]. Vall-Ilosera *et al.*[51] attributed these features to the excitations to Rydberg or mixed valence-Rydberg orbitals with some antibonding character of both σ* and π* symmetries.

The experimental N $1s^{-1}$ CEBE determined from the yield of high-Rydberg fragments equals 406.5 eV. This value is in agreement with all theoretical results. Indeed, our calculated value is 0.22 eV lower than the experimental one (see Table 4). The DFT result of Chong and Hu[18] is only 0.11 eV lower, while that calculated by Du *et al.*[19] differs by 0.45 eV. The condensed phase measurement result is lower by about 4 eV than our gas-phase value.

3.3. O K-edge

The O 1s NEXAFS spectrum of isoxazole was measured in the 529-540 eV energy range with 100 meV steps (see Figure 4). There was some residual O_2 in the chamber due to a small leak in the gas inlet system so that the O(1s)$\rightarrow\pi^*$ transition of the O_2 molecule is visible below the first resonance in Figure 4 as a small structure at 530.8 eV. The energy calibration was performed according to this transition.

The experimental spectrum consists of one strong peak and a broad absorption band centered around 538 eV. The calculations indicate that the two lowest theoretical transitions are the most intense ones, similarly to the N 1s NEXAFS. The first core excitation is predicted at 534.92 eV and corresponds to the O(1s) $\rightarrow$ 4a'' (LUMO) excitation. It correlates well with the sharp experimental peak at 534.60 eV. The tiny peak at 535.37 eV likely derives from the vibrational fine structure of this excitation.

The experimental spectrum is quite broad in the 536-541 eV energy range, so the present decomposition is tentative. A noticeable peak given by simulations at 536.33 eV has no counterpart in the theoretical spectrum. The second major transition is a core-Rydberg transition centered at 537.49 eV, whose main contributions are analogous to the second core-excited state in the N 1s spectrum. This transition can be correlated to the broad absorption hump centered at 537.46 eV. A large band at 539.34 eV in the O 1s NEXAFS spectrum likely consists of the

O(1s)→3s and O(1s)→5a'' (Figure 5) excitations, and the O(1s)→3p$_y$ core-Rydberg transition (538.72 eV).

As given in Table 4, the experimental O 1s^{-1} CEBE was estimated from the high-Rydberg yield to be at 540.4 eV. Our calculated value is 0.39 eV lower, while the DFT result of Chong and Hu[18] is 0.3 eV higher than our experimental value. The result from the condensed phase measurement[17] is lower by about 4 eV, similarly to the N 1s^{-1} CEBE.

3.4. Vibrationally resolved spectra of isoxazole

As seen in Table 5, the GS, O 1s, and N 1s minima retain the exact planarity (the C_s symmetry), whereas all three C 1s minima end up slightly non-planar. In all cases, the dominant single contribution is due to the 1s → π*(LUMO) excitation with the corresponding weights in the range of 0.6-0.7. The changes in the geometries relative to the GS are the net result of a complex interplay of the presence of the core-hole and the population of the antibonding LUMO and several of the low-lying diffuse MOs. The O 1s structure is the only one that undergoes a complete scission of the N-O bond. Indeed, the N-O distance extends here to more than 2 Å, but all the atoms remain in the same plane. Consequently, in this case, the LUMO lies in-plane (the A' symmetry) and involves the σ*(N-O) antibonding interaction.

Conversely, in the N 1s and the three C 1s minima, the LUMO retains the π* character. However, because of the structural relaxation, its appearance is somewhat different from the 4a'' (LUMO) in Figure 5. For example, common to both the N 1s and C 1s minima is the C3-C4 bond shortening relative to the GS, which is reflected in the C3-C4 bonding interaction seen in the LUMO. The population of the LUMO weakens the resonant aromatic stabilization and thus reduces the barrier to the deplanarization of the isoxazole ring.

The FCHT model reasonably reproduces the features of the low-lying bands, and the computed vibronic progressions correlate well with various peaks and shoulders observed in the

16

C 1s and N 1s NEXAFS (see Figures 7 and 8). The model failed to produce spectrum only in the case of the lowest O 1s root owing to the breakdown of the FC approximation. This usually occurs when significant differences between the ground and excited-state geometries are encountered, which in this particular case can be attributed to the N-O bond scission in the first O 1s core-excited state (Table 5).

Considering that the different methods were used to produce the ground state and core-excited state minima and harmonic frequencies (i.e. MP2 and $BH^{0.58}LYP$) the absolute positions of the band origins (0-0) are not useful. For this reason, the computed vibrationally resolved spectra had to be shifted, and this was done in such a way that the strongest predicted vibronic transition matches the strongest observed peak within a given band. We emphasize, however, that in case of the C 1s NEXAFS we did not change the predicted relative difference between the C3 1s and C5 1s band origins (E_{0-0} (C5 1s) − E_{0-0} (C3 1s) = 0.46 eV). Therefore, the FCHT model nicely correlates the two peaks measured at 285.8 and 286.4 eV (Figure 7) to the most intense vibronic transitions originating from the C3 1s and C5 1s cores, namely 2 and 8 (Figure 7). Thus, unlike the N 1s case, the 0-0 transitions are not the strongest one in the C 1s NEXAFS, which gives rise to the interesting spectral features on both high- and low-energy sides of the two central peaks. The modes that contribute most to the C3 1s and C5 1s vibronic spectra are the out-of-plane wagging of the H atoms. This puckers the ring leading to the deplanarization and the twisted (half-chair) conformation typical of 5-membered organic rings.

On the other hand, the larger discrepancies between the ground state and C4 1s minimum geometries, in particular, due to the more pronounced deplanarization of the ring (Table 5), result in a relatively low-intensity 0-0 origin in this case. Consequently, the FCHT approximation is not sufficiently justified, and the percentage spectrum progression remains comparatively low. Hence in Figure 7, we omit the detailed assignment of the C4 1s spectrum.

The relative ordering of the C atoms by the vertical and adiabatic core-excitation energies, the latter obtained from the root-specific optimizations, remains the same (C4 < C3 < C5; Figure 7). As is also the case with the vertical C 1s spectrum, there are no significant mixings of the single excitations from the C 1s cores on different centers.

The FCHT computations provide further evidence that the lowest C4 1s and C3 1s transitions are insufficiently resolved in the vertical SRC2-BLYP spectra. Furthermore, there exists a mismatch between the positions of the vertical TD-DFT transitions (i.e., when computations are done on a fixed geometry) and the strongest vibronic transitions. Specifically, the C3 1s and C5 1s maxima are more apart in the vibrationally resolved spectrum. These occurrences make it difficult to accurately assign the low-lying C 1s NEXAFS region (Figure 7) based on the vertical spectra alone and hint at why the SRC2-BLYP spectrum necessitates the red shift of −0.5 eV to achieve a better overlap with the measured lowest bands (Figure 2).

The vibrationally resolved C 1s photoelectron spectrum measured in isoelectronic furan also displayed vibrational progression[52]. The *ab initio* calculations of the vibrational coupling constants within the linear coupling model were performed to elucidate the resulting structures. These calculations revealed six major vibrational modes playing a role in the experimental spectrum shape: a localized C-H stretching vibration and the others were ring deformations or mixtures of ring deformations with C-H angle bends[52].

The vibrationally resolved core-excited spectra of isoxazole can also be compared to another molecule containing a 5-ring, catecholborane[53]. Comparing the fine structure of the lowest C 1s and B 1s bands, the isoxazole spectra are more complex with the significant involvement of many low-lying out-of-plane vibrational modes. The reason is the greater flexibility of the isoxazole ring as in catecholborane the 5-ring is fused to the benzene core. Consequently, the puckering of the isoxazole ring promoting the half-chair conformation

MOST WIEDZY Downloaded from mostwiedzy.pl

becomes feasible, whereas in catecholborane, usually, only the simpler B-envelope conformation is present.

In the vibrationally resolved N 1s spectrum, the 0-0 transition is the most intense by far, which matches the general appearance of the band. The vibronic progressions are dominated by the excitation of an in-plane A' symmetric vibrational mode involving mainly the C4-C5 stretch (Figures 8 and 9). In general, the most prominent vibrational modes faithfully reflect the geometric changes that need to occur when going from the ground state to a given core-excited minimum.

4. Conclusions

We have investigated the NEXAFS spectra of isoxazole at the C, N, and O K-edges through experiments and calculations. The C 1s spectrum contains well-resolved features and is quite complex because there are three chemically nonequivalent C atoms in isoxazole. On the contrary, the N 1s and O 1s spectra seem to be less complex consisting of prominent first peaks followed by wide bands. However, their complexity is hidden in unresolved features.

The computational TD-DFT predictions of the NEXAFS spectra cover the excitations of the 1s electrons to the low-lying valence and Rydberg states, up to the vicinity of the core-ionization thresholds. In all cases, the states involved are of singlet character. The lowest-lying major transitions correspond predominantly to the (1s)$\rightarrow$4a" (LUMO) excitations. In the case of C 1s, these excitations reveal a well-separated vibrational fine structure. The remaining transitions are the (1s)$\rightarrow$5a" core-valence transitions and the (1s)$\rightarrow$3s core-Rydberg transitions with a notable contribution of the in-plane 3p Rydberg orbital (1s)$\rightarrow$3p$_y$.

It can be concluded that consideration of the vertical TD-DFT spectrum alone is insufficient for an unambiguous assignment of the unusually complex C 1s NEXAFS. Thus, the analogous uncertainties, in particular for the lowest C 1s bands, are maintained on employing the

two modern density functionals in the framework of TD-DFT, viz. SRC2-BLYP and M06-2X. Consequently, a better description of the XPS and NEXAFS spectra of isoxazole should go beyond the vertical TD-DFT picture. To this end, we computed the vibrationally resolved spectra in the FCHT framework using the MP2 and TD-DFT minima and harmonic frequencies for the ground state and the first core-excited roots. This model successfully produced the vibronic envelopes for the lowest C 1s and N 1s bands but not for the O 1s case. Especially for the C 1s NEXAFS, the FCHT procedure proved helpful in resolving several ambiguities in the assignment of the low-lying transitions that arose from the SRC2-BLYP vertical spectrum. The spectral features of the FCHT and measured vibronic bands are generally in reasonable agreement.

We have also provided the experimental C 1s, N 1s, and O 1s CEBEs of the isoxazole determined from the yields of high-Rydberg fragments. For comparison, theoretical CEBEs have additionally been calculated. Theoretical predictions and experimental results are in excellent agreement suggesting that the yield measurement of high-Rydberg fragments provides a simple technique to determine core electron binding energies quite accurately if a photoelectron spectrometer is not available. However, our experimental CEBEs should be confirmed by measuring core-level photoelectron spectra of the isoxazole molecule.

Notes

The authors declare no competing financial interest.

References

1. M. Zubek, T. J. Wasowicz, I. Dąbkowska, A. Kivimäki, M. Coreno, Hydrogen Migration in Formation of $NH(A^3\Pi)$ Radicals Via Superexcited States in Photodissociation of Isoxazole Molecules. *J. Chem. Phys.* 2014, **141**, 064301, DOI: 10.1063/1.4891808

2. J. Zhu, J. Mo, H.-Z. Lin, Y. Chen, H.-P. Sun, The Recent Progress of Isoxazole in Medicinal Chemistry. *Bioorg. Med. Chem.* 2018, *26*, 3065–3075, DOI: 10.1016/j.bmc.2018.05.013

3. C. Lamberth, Oxazole and Isoxazole Chemistry in Crop Protection. *J. Heterocycl. Chem.* 2018, **55**, 2035– 2045, DOI: 10.1002/jhet.3252

4. A. Sysak, B. Obmińska-Mrukowicz, Isoxazole Ring as a Useful Scaffold in a Search for New Therapeutic Agents. *Eur. J. Med. Chem.* 2017, **137**, 292–309, DOI: 10.1016/j.ejmech.2017.06.002

5. M. Zimecki, U. Bachor, M. Maczyński, Isoxazole Derivatives as Regulators of Immune Functions. *Molecules* 2018, **23**, 2724, DOI: 10.3390/molecules23102724

6. D. J. Burkhart, N. R. Natale, Isoxazole Ionotropic Glutamate Neurotransmitters. *Curr. Med. Chem.* 2005, **12**, 617-627, DOI: 10.2174/0929867053362893

7. H. Wang, Y. Ma, Y. Lin, J. Liu, R. Chen, B. Xu, Y. Liang, An Isoxazole Derivative SHU00238 Suppresses Colorectal Cancer Growth Through miRNAs Regulation. *Molecules* 2019, **24**, 2335, DOI: 10.3390/molecules24122335

21

8. I. C. Walker, M. H. Palmer, J. Delwiche, S. V. Hoffmann, P. L. Vieora, N. J. Mason, M. F. Guest, M.-J. Hubin-Franskin, J. Heinesch, A. Giuliani, The Electronic States of Isoxazole Studied by V.U.V. Absorption, Electron Energy-loss Spectroscopies and Ab Initio Multi-reference Configuration Interaction Calculations. *Chem. Phys.* 2004, **297**, 289–306, DOI: 10.1016/j.chemphys.2003.10.012

9. J. Cao, Photoinduced Reactions of Both 2-Formyl-2h-Azirine and Isoxazole: A Theoretical Study Based on Electronic Structure Calculations and Nonadiabatic Dynamics Simulations. *J. Chem. Phys.* 2015, **142**, 244302, DOI: 10.1063/1.4922742

10. T. J. Wasowicz, A. Kivimäki, M. Coreno, M. Zubek, Superexcited States in the Vacuum-Ultraviolet Photofragmentation of Isoxazole Molecules. *J. Phys. B: At. Mol. Opt. Phys.* 2012, **45**, 205103, DOI: 10.1088/0953-4075/45/20/205103

11. I. Linert, I. Lachowicz, T. J. Wasowicz, M. Zubek, Fragmentation of Isoxazole Molecules by Electron Impact in the Energy Range 10–85 eV. *Chem. Phys. Lett.* 2010, **498**, 27– 31, DOI: 10.1016/j.cplett.2010.08.034

12. Z. Li, I. Carmichael, S. Ptasińska, Dissociative Electron Attachment Induced Ring Opening in Five-membered Heterocyclic Compounds. *Phys. Chem. Chem. Phys.* 2018, **20**, 18271–18278, DOI: 10.1039/C8CP02718H.

13. A. A. Wallace, Y. Dauletyarov, A. Sanov, Deprotonation of Isoxazole: A Photoelectron Imaging Study. *J. Phys. Chem. A* 2020, **124**, 7768–7775, DOI: 10.1021/acs.jpca.0c06838

14. T. Geng, J. Ehrmaier, O. Schalk, G. W. Richings, T. Hansson, G. Worth, R. D. Thomas, Time-Resolved Photoelectron Spectroscopy Studies of Isoxazole and Oxazole. *J. Phys. Chem. A* 2020, **124**, 3984– 3992, DOI: 10.1021/acs.jpca.9b11788

15. T. J. Wasowicz, A. Kivimäki, D. Catone, R. Richter, Vacuum Ultraviolet Photoionization and Ionic Fragmentation of the Isoxazole Molecules. *Int. J. Mass Spectrom.* 2020, **449**, 116276, DOI: 10.1016/j.ijms.2019.116276

16. T. Jani, A. Shastri, D. Prajapati, P. C. Vinodkumar, C. Limbachiya, M. Vinodkumar, Structural, Spectroscopic and Electron Collisional Studies of Isoxazole (C_3H_3NO). *Chem. Phys.* 2022, **553**, 111379, DOI: 10.1016/j.chemphys.2021.111379

17. D. T. Clark, D. M. J. Lilley, Molecular Core Binding Energies for Some Five Membered Ring Heterocycles as Determined by X-Ray Photoelectron Spectroscopy. *Chem. Phys. Lett.* 1971, **9**, 234-237, DOI: 10.1016/0009-2614(71)85038-8

18. D. P. Chong, C.-H. Hu, Accurate density functional calculation of core-electron binding energies with a scaled polarized triple-zeta basis set. IV. Application to isomers of C_3H_6O, C_3H_3NO, and C_6H_6. *J. Chem. Phys.* 1998, **108**, 8950-8956, DOI: 10.1063/1.476340

19. X. Du, S.-Y. Wang, M. Wei, J.-R. Zhang, G. Ge, W. Hua, A Theoretical Library of N 1s Core Binding Energies of Polynitrogen Molecules and Ions in the Gas Phase. *Phys. Chem. Chem. Phys.* 2022, DOI: 10.1039/D2CP00069E

20. N. A. Besley, M. J. G. Peach, D. J. Tozer, Time-dependent density functional theory calculations of near-edge X-ray absorption fine structure with short-range corrected functionals. *Phys. Chem. Chem. Phys.* 2009, **11**, 10350-10358.

21. K. C. Prince, R. R. Blyth, R. Delaunay, M. Zitnik, J. Krempasky, J. Slevak, R. Camilloni, L. Avaldi, M. Coreno, G. Stefani, C. Furlani, The Gas-Phase Photoemission Beamline at Elettra. *J. Synchtrotron Radiat.* 1998, **5**, 565–568, DOI: 10.1107/S090904959800065X

22. A. Kivimäki, A. Sankari, J. A. Kettunen, C. Stråhlman, J. Álvarez Ruiz, R. Richter, Field Ionization of High-Rydberg Fragments Produced after Inner-Shell Photoexcitation and Photoionization of the Methane Molecule. *J. Chem. Phys.* 2015, **143**, 114305, DOI: 10.1063/1.4931105

23. A. Kivimäki, C. Stråhlman, T. J. Wasowicz, J. A. Kettunen, R. Richter, Yields and Time-of-Flight Spectra of Neutral High-Rydberg Fragments at the K Edges of the CO_2 Molecule. *J. Phys. Chem. A.* 2016, **120**, 4360– 4367, DOI: 10.1021/acs.jpca.6b04495

24. R. N. Sodhi, C. E. Brion, Reference Energies for Inner Shell Electron Energy-loss Spectroscopy. *J. Electron Spectrosc. Rel. Phenom.* 1984, **34** (4), 363-372, DOI: 10.1016/0368-2048(84)80050-X

25. A. P. Hitchcock, C. E. Brion, K-shell Excitation Spectra of C.O., N_2 and O_2. *J. Electron Spectrosc. Rel. Phenom.* 1980, **18** (1), 1-21. DOI: 10.1016/0368-2048(80)80001-6

26. CSID:8897, http://www.chemspider.com/Chemical-Structure.8897.html (accessed 15:21, March 08, 2022)

27. M. J. Frisch, M. Head-Gordon, J. A. Pople, A direct MP2 gradient method. *Chem. Phys. Lett.* 1990, **166**, 275-280.

28. T. H. Dunning Jr., Gaussian basis sets for use in correlated molecular calculations. I. The atoms boron through neon and hydrogen. *J. Chem. Phys.* 1989, **90**, 1007-1023.

29. Y. Zhao, D. G. Truhlar, The M06 suite of density functionals for main group thermochemistry, thermochemical kinetics, noncovalent interactions, excited states, and transition elements: two new functionals and systematic testing of four M06-class functionals and 12 other functionals. *Theor. Chem. Acc.* 2008, **120**, 215-241.

30. B. Kovač, I. Ljubić, A. Kivimäki, M. Coreno, I. Novak, The study of the electronic structure of some N-heterocyclic carbenes (NHCs) by variable energy photoelectron spectroscopy. *Phys. Chem. Chem. Phys.* 2015, **17**, 10656-10667.

31. J. Shim, M. Klobukowski, M. Barysz, J. Leszczynski, Calibration and applications of the ΔMP2 method for calculating core electron binding energies. *Phys. Chem. Chem. Phys.* 2011, **13**, 5703-5711.

32. K. A. Peterson, T. H. Dunning Jr, Accurate correlation consistent basis sets for molecular core–valence correlation effects: The second row atoms Al–Ar, and the first row atoms B–Ne revisited. *J. Chem. Phys.* 2002, **117**, 10548.

33. E. Miyoshi, H. Mori, R. Hirayama, Y. Osanai, T. Noro, H. Honda, M. Klobukowski, Compact and efficient basis sets of *s*- and *p*-block elements for model core potential method. *J. Chem. Phys.* 2005, **122**, 074104.

34. I. Ljubić, Reliability of density functional and perturbation theories for calculating core-ionization spectra of free radicals. *J. Chem. Theory Comput.* 2014, **10**, 2333-2343.

35. A. T. B. Gilbert, N. A. Besley, P. M. W. Gill, Self-Consistent Field Calculations of Excited States Using the Maximum Overlap Method (MOM). *J. Phys. Chem. A* 2008, **112**, 13164-13171.

36. N. A. Besley, A. T. Gilbert, P. M. Gill, Self-Consistent-Field Calculations of Core-Excited States. *J. Chem. Phys.* 2009, **130**, 124308, DOI: 10.1063/1.3092928.

37. N. A. Besley, Density Functional Theory Based Methods for the Calculation of X-ray Spectroscopy. *Acc. Chem. Res.* 2020, **53**, 1306–1315.

38. S. Hirata, M. Head-Gordon, Time-dependent density functional theory within the Tamm–Dancoff approximation, *Chem. Phys. Lett.*, 1999, **314**, 291-299.

39. N. A. Besley, F. Asmuruf, Time-dependent density functional theory calculations of the spectroscopy of core electrons. *Phys. Chem. Chem. Phys.*, 2010, **12**, 12024-12039.

40. I. Ljubić, A. Kivimäki, M. Coreno, An experimental NEXAFS and computational TDDFT and ΔDFT study of the gas-phase core excitation spectra of nitroxide free radical TEMPO and its analogues. *Phys. Chem. Chem. Phys.*, 2016, **18**, 10207-10217.

41. F. Santoro, A. Lami, R. Improta, J. Bloino, V. Barone, Effective method for the computation of optical spectra of large molecules at finite temperature including the Duschinsky and Herzberg–Teller effect: The Qx band of porphyrin as a case study. *J. Chem. Phys.* 2008, **128**, 224311.

42. M. J. Frisch, *et al.* Gaussian 16, Revision C.01, Gaussian, Inc., Wallingford CT, 2019.

43. G. M. J. Barca, *et al.* Recent developments in the general atomic and molecular electronic structure system. *J. Chem. Phys.* 2020, **152**, 154102.

44. Y. Shao, *et al.* Advances in molecular quantum chemistry contained in the Q-Chem 4 program package. *Mol. Phys.* 2015, **113**, 184-215.

45. G. Schaftenaar, J.H. Noordik, Molden: a Pre- and Post-processing Program for Molecular and Electronic Structures. *J. Comp.-Aided Mol. Design* 2000, **14**, 123–134, DOI: 10.1023/A:1008193805436

46. Y. Hikosaka, P. Lablanquie, E. Shigemasa, Efficient Production of Metastable Fragments around the 1s Ionization Threshold in N_2. *J. Phys. B: At., Mol. Opt. Phys.* 2005, **38**, 3597–3605, DOI: 10.1088/0953-4075/38/19/012

47. A. Kivimäki, T.J. Wasowicz, R. Richter, Soft X-ray Induced Production of Neutral Fragments in High-Rydberg States at the O 1s Ionization Threshold of the Water Molecule. *J. Phys. Chem. A.* 2021, **125**, 713–720, DOI: 10.1021/acs.jpca.0c06940

48. D. Duflot, J.-P. Flament, A. Giuliani, J. Heinesch, M.-J. Hubin-Franskin, Core shell excitation of furan at the O 1s and C 1s edges: An experimental and ab initio study. *J. Chem. Phys.* 2003, **119**, 8946– 8955, DOI: 10.1063/1.1606441

49. B. O. Roos, R. Lindh, P-Å Malmqvist, V. Veryazov, P.-O. Widmark, Multiconfigurational Quantum Chemistry, John Wiley & Sons, Hoboken, New Jersey, 2016, pp. 172-179.

50. A. Chantzis, A. D. Laurent, C. Adamo, D. Jacquemin, Is the Tamm-Dancoff Approximation Reliable for the Calculation of Absorption and Fluorescence Band Shapes?, *J. Chem. Theory Comput.* 2013, **9**, 4517–4525.

51. G. Vall-Llosera, G. Gao, A. Kivimäki, M. Coreno, J. Álvarez Ruiz, M. de Simone, H. Ågren, E. Rachlew, The C 1s and N 1s Near Edge X-Ray Absorption Fine Structure Spectra of Five Azabenzenes in the Gas Phase. *J. Chem. Phys.* 2008, **128**, 044316 DOI: 10.1063/1.2822985

52. E. E. Rennie, U. Hergenhahn, O. Kugeler, A. Rüdel, S. Marburger, A. M. Bradshaw, A Core-Level Photoionization Study of Furan. *J. Chem. Phys.* 2002, **117** (14), 6524– 6532, DOI: 10.1063/1.1504435

53. I. Ljubić, M. T. Cvitaš, C. Grazioli, M. Coreno, S. Kazazić, I. Novak, Vibrationally resolved valence and core photoionization and photoexcitation spectra of an electron-deficient trivalent boron compound: the case of catecholborane. *Phys. Chem. Chem. Phys.* 2020, **22**, 25396-25407.
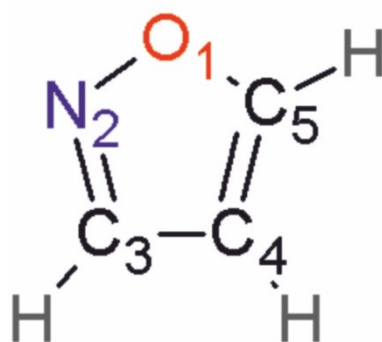
Figure 1. Schematic diagram of the isoxazole molecule, C_3H_3NO, showing labeling of the atoms.
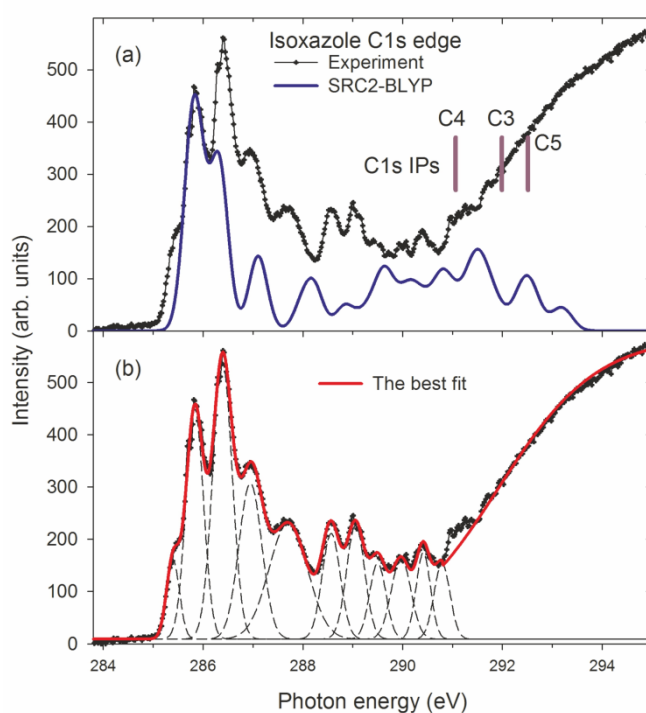

Figure 2. (a) Experimental and theoretical C 1s NEXAFS spectra of isoxazole. The theoretical spectrum was shifted by –0.5 eV. The vertical bars represent ionization potentials determined experimentally in the present work. (b) Result of a least-squares fitting. The dashed lines show the bands fitted to the experimental curve, and the solid red line shows the final fit.
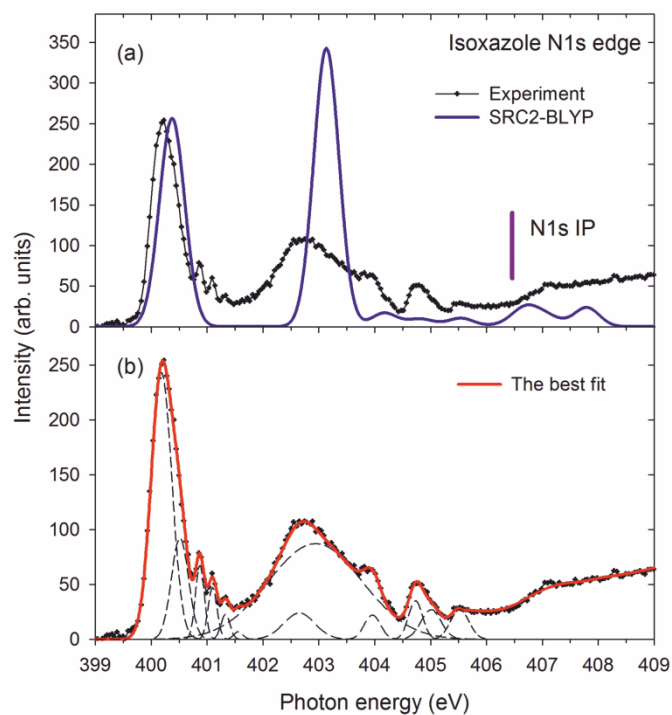
Figure 3. (a) Experimental and theoretical N 1s NEXAFS spectra of isoxazole. Narrow peaks around 401 eV are due to the N 1s$\rightarrow\pi^*$ transitions in N_2. The vertical bar represents ionization potential determined experimentally in the present work. (b) Result of a least-squares fitting. The dashed lines show the bands fitted to the experimental curve, and the solid red line shows the final fit.
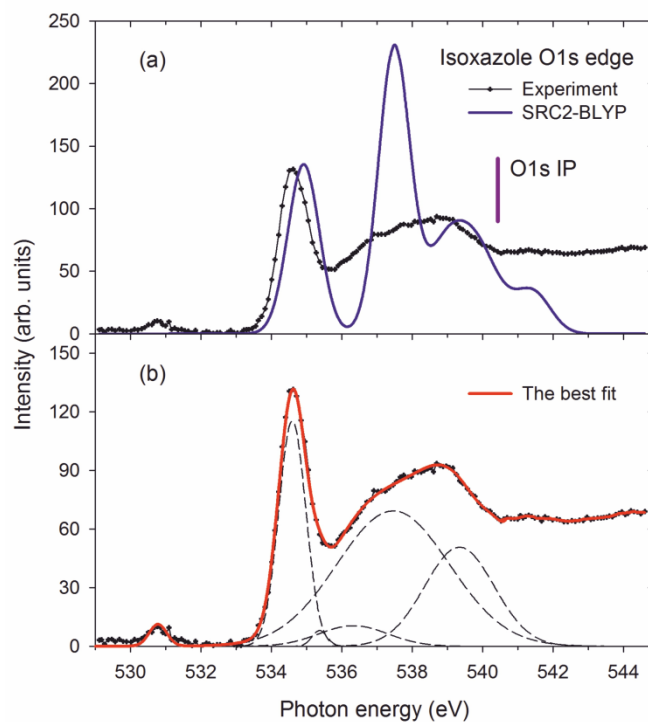
Figure 4. (a) Experimental and theoretical O 1s NEXAFS spectra of isoxazole. The feature at ~530.8 eV is due to the O 1s→π* transitions in O_2. The vertical bar represents ionization potential determined experimentally in the present work. (b) Result of a least-squares fitting. The dashed lines show the bands fitted to the experimental curve, and the solid red line shows the final fit.

4a'' (LUMO)

6a'' (3p$_z$)

16a' (3s)

19a' (3d$_{xy}$)

17a' (3p$_y$)

20a' (3d$_{x^2-y^2}$)

5a'' (π*(C-C))

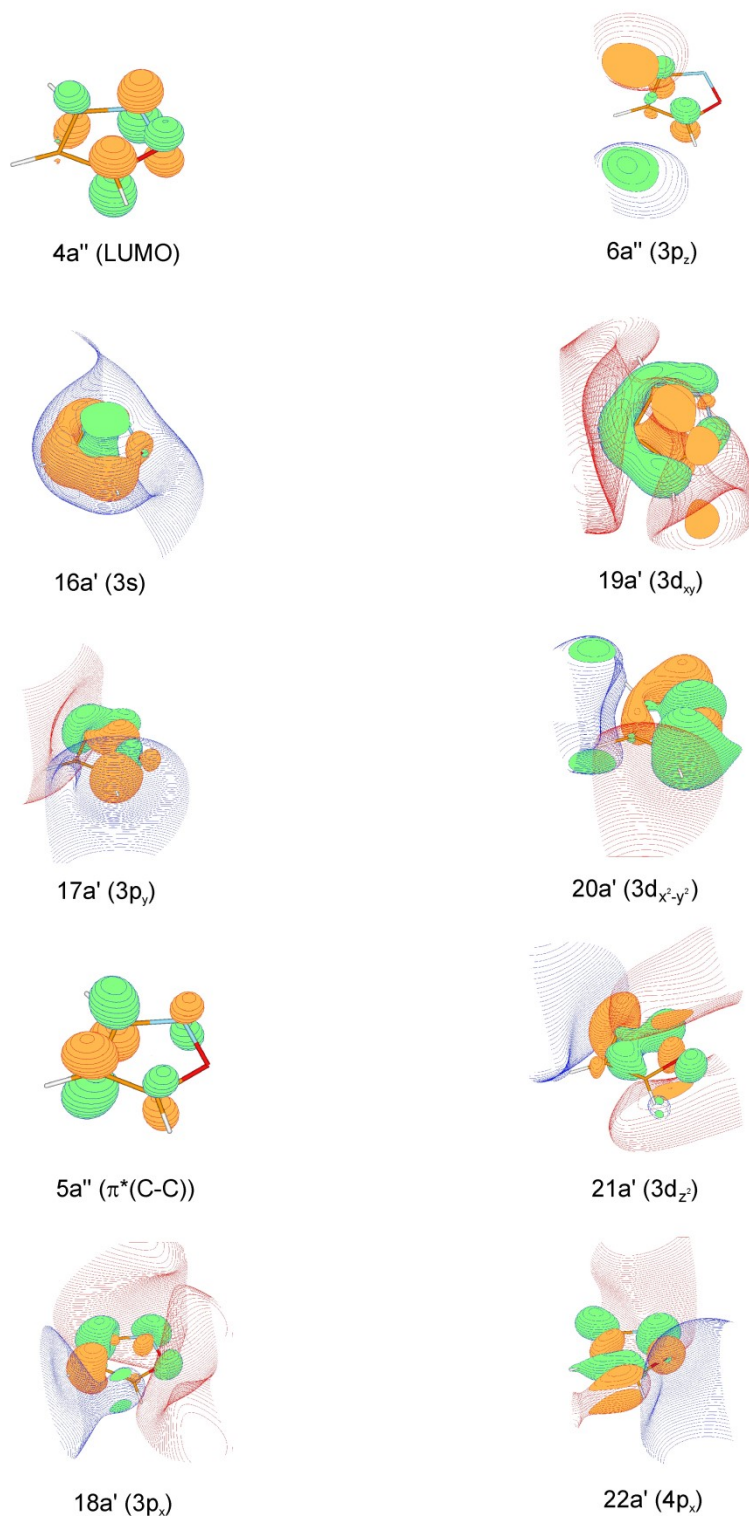21a' (3d$_{z^2}$)

18a' (3p$_x$)

22a' (4p$_x$)

Figure 5. Ten lowest virtual orbitals of isoxazole at the SRC2-BLYP/6-311(2+,2+)G** level.
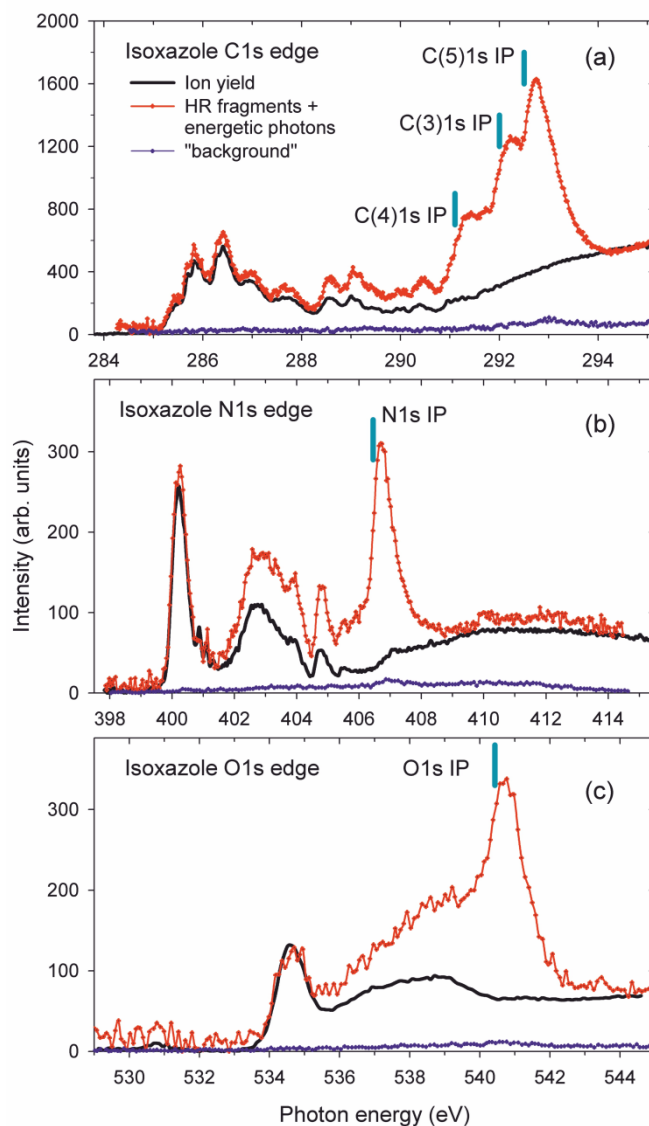
Figure 6. Different particle yields measured at the K-edges of the isoxazole molecule. The red crosshair curves show the sum of field-ionized HR fragments, neutral metastable fragments, and photons. The solid black line shows the NEXAFS spectra. The navy blue dotted contours depict the sum of neutral metastable fragments and photons without field ionization. The C/N/O 1s ionization potentials (the vertical bars) have been estimated based on the energy of the above-threshold peaks in the yields of HR fragments.
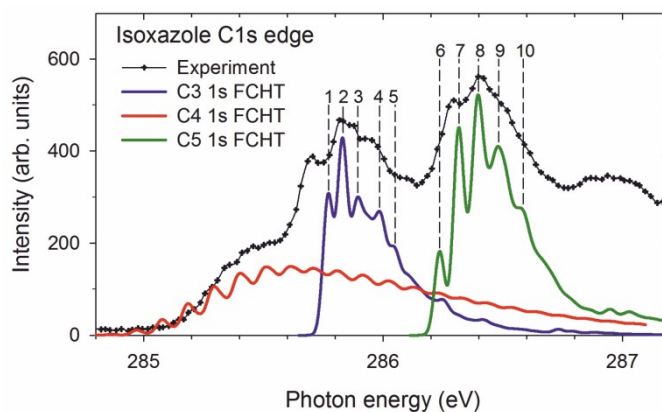
Figure 7. The vibrationally resolved FCHT spectrum superimposed on the lowest C 1s NEXAFS bands region. The Gaussian line shapes are used with the FWHM parameter set to 400 cm^{-1} (49.6 meV). The most prominent contributions to the vibronic progressions are for C3 1s: **1** = 0-0; **2** = 2_0^1; **3** = 2_0^2 + 11_0^1; **4** = $(11_0^1; 2_0^1)$; **5** = $(12_0^1; 2_0^1)$ + $(15_0^1; 2_0^1)$; and for C5 1s: **6** = 0-0; **7** = 3_0^1 + 4_0^1; **8** = $(4_0^1; 3_0^1)$ + 4_0^2; **9** = $(4_0^1; 3_0^2)$ + $(4_0^2; 3_0^1)$; **10** = $(4_0^1; 3_0^2; 6_0^1)$.

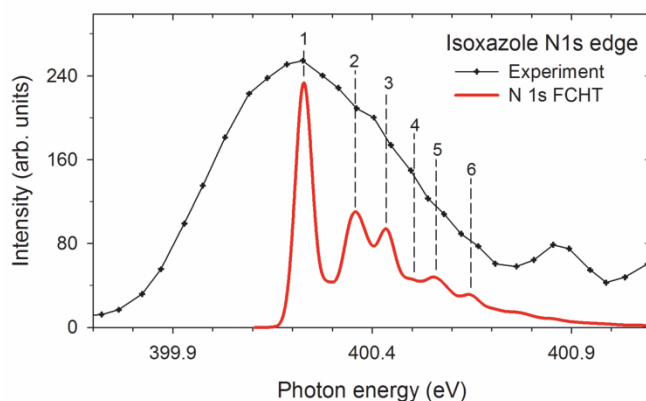Figure 8. The vibrationally resolved FCHT spectrum superimposed on the lowest N 1s NEXAFS band region. The Gaussian line shapes are used with the FWHM parameter set to 400 cm^{-1}. The most prominent contributions to the vibronic progressions are: **1** = 0-0 + 1_0^2 ; **2** = 6_0^1 + 10_0^1 + 11_0^1; **3** = 15_0^1; **4** = $(15_0^1; 1_0^2)$; **5** = $(15_0^1; 6_0^1)$; **6** = 15_0^2.
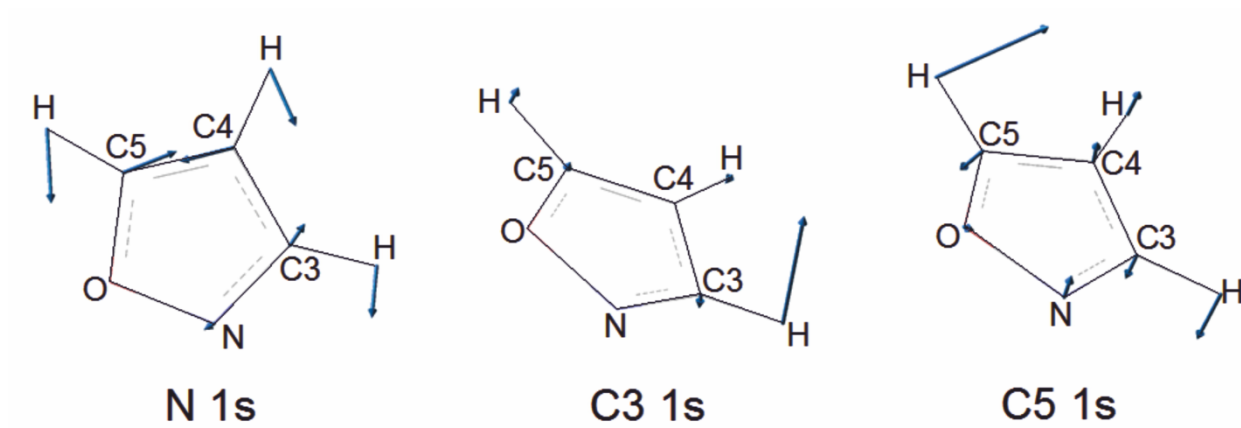
Figure 9. The vibrational modes that give rise to the largest intensities in the FCHT spectra: (a) N 1s; $15_0^1 = 1678$ cm^{-1}; (b) C3 1s; $2_0^1 = 475$ cm^{-1}; (c) C5 1s; $4_0^1 = 661$ cm^{-1}.

Table 1. The experimental (E_{exp}) and calculated (E_{th}) energies and assignments of the C 1s core-excited states of isoxazole. The calculated oscillator strengths (f) and squared amplitudes (A^2) of particular transitions are also given. Calculated energies were shifted by –0.5 eV.

No.	E_{exp} (eV)	E_{th} (eV)	Assignment			f	A^2
			C3	C4	C5		
1	285.40	285.75		C(1s)→4a''(LUMO) C(1s)→5a''		0.0351	0.76 0.21
2	285.83	285.87	C(1s)→4a''(LUMO) C(1s)→5a''			0.0542	0.76 0.20
3	286.39	286.32			C(1s)→4a''(LUMO) C(1s)→5a''	0.0620	0.88 0.09
4	286.95	287.10		C(1s)→5a'' C(1s)→4a''(LUMO)		0.0275	0.72 0.24
5	287.70	287.99		C(1s)→3s		0.0085	0.90
6	288.57	288.23	C(1s)→5a'' C(1s)→4a''(LUMO)			0.0150	0.74 0.23
7	289.06	288.83	C(1s)→3s C(1s)→3p$_y$			0.0072	0.81 0.10
8	289.50	289.63			C(1s)→3s C(1s)→3p$_y$	0.0113	0.81 0.08
9	289.97	289.65			C(1s)→5a'' C(1s)→4a''(LUMO)	0.0060	0.86 0.10
10	290.41						

Table 2. The experimental (E_exp) and calculated (E_th) energies and assignments of the N 1s core-excited states of isoxazole. The calculated oscillator strengths (*f*) and squared amplitudes (A^2) of particular transitions are also given.

No.	E_exp (eV)	E_th (eV)	Assignment	f	A^2
1	400.19 400.52	400.38	N(1s)→4a''(LUMO) N(1s)→5a''	0.0553	0.88 0.09
2	402.65				
3	402.94	403.14	N(1s)→3d$_{x2-y2}$ → LUMO + 16 → LUMO + 17 → LUMO + 18 → LUMO + 25 → LUMO + 26	0.0739	0.08 0.18 0.06 0.13 0.11 0.14
4	403.96	404.16	N(1s)→4a''(LUMO) N(1s)→5a''	0.0034	0.10 0.90
5	404.73				
6	405.01				
7	405.52				

Table 3. Experimental (E_{exp}) and calculated (E_{th}) energies and assignments of the O 1s core-excited states of isoxazole. The calculated oscillator strengths (f) and squared amplitudes (A^2) of particular transitions are also given.

No.	E_{exp} (eV)	E_{th} (eV)	Assignment	f	A^2
1	534.60 535.37	534.92	O(1s)→4a''(LUMO)	0.0305	0.98
2	536.33				
3	537.46	537.49	O(1s)→ 3d$_{x2-y2}$ → LUMO + 16 → LUMO + 17 → LUMO + 18 → LUMO + 25 → LUMO + 26	0.0515	0.05 0.12 0.05 0.18 0.18 0.08
4	539.34	538.34 538.44 538.72	O(1s)→3s O(1s)→5a'' O(1s)→3p$_y$	0.0012 0.0002 0.0084	0.96 0.99 0.85

Table 4. Experimental (E_{exp}) and calculated (E_{th}) core electron binding energies (in eV). E_{th} was calculated at the ΔM06-2X//mixed basis set level (cc-pwCVTZ on the atom whose CEBE is calculated; mcp-DZP on the remaining second-row atoms; cc-pVDZ on H atoms). Relativistic corrections (RC) were applied as recommended in[36] (+0.1 eV for C, +0.21 for N, and +0.36 eV for O atoms).

	C3	C4	C5	N	O
E_{exp} (±0.2)	292.0	291.1	292.5	406.5	540.4
E_{th} (ΔM06-2X)	291.80	290.95	292.50	406.07	539.65
E_{th} (RC)	291.90	291.05	292.60	406.28	540.01
E_{exp} (±0.3)[17]	286.9	285.9	287.4	402.1	536.6
E_{th}[18]	292.00	291.30	292.62	406.39	540.70
E_{th} (±0.30)[19]				406.05	

Table 5. Geometric parameters of the ground state (GS) (the BH[0.58]LYP/6-311+G(2d,p) and MP2/cc-pVTZ levels) and the lowest core-excited roots (the TD-BH[0.58]LYP/6-311+G(2d,p) level). The distances are given in Å; the dihedral angle in °. The enumeration of the C atoms follows Figure 1.

	GS BH[0.58]LYP	GS MP2	O 1s	N 1s	C3 1s	C4 1s	C5 1s
N-O	1.364	1.380	2.064	1.341	1.417	1.352	1.411
C3-N	1.285	1.323	1.220	1.321	1.319	1.262	1.288
C5-O	1.320	1.345	1.340	1.380	1.321	1.390	1.336
C3-C4	1.414	1.411	1.517	1.403	1.396	1.385	1.386
C4-C5	1.338	1.362	1.281	1.327	1.322	1.362	1.361
C3-N-O-C5	0.0	0.0	0.0	0.0	3.8	5.4	3.2

Graphical Table of Contents